Sciencexpress Reports

Shear-Activated Nanotherapeutics for Drug Targeting to Obstructed Blood Vessels

Netanel Korin,[1] Mathumai Kanapathipillai,[1] Benjamin D. Matthews,[2,3] Marilena Crescente,[4,5] Alexander Brill,[4,5] Tadanori Mammoto,[2] Kaustabh Ghosh,[2] Samuel Jurek,[2] Sidi A. Bencherif,[1,6] Deen Bhatta,[6] Ahmet U. Coskun,[7] Charles L. Feldman,[8] Denisa D. Wagner,[4,5] Donald E. Ingber[1,2,6]*

[1]Wyss Institute for Biologically Inspired Engineering at Harvard University, Boston, MA 02115, USA. [2]Vascular Biology Program, Departments of Pathology and Surgery, Children's Hospital Boston, and Harvard Medical School, Boston, MA 02115, USA. [3]Department of Medicine, Children's Hospital Boston, and Harvard Medical School, Boston, MA 02115, USA. [4]Immune Disease Institute, Program in Cellular and Molecular Medicine, Children's Hospital Boston, Boston, MA, USA. [5]Department of Pediatrics, Harvard Medical School, Boston, MA, USA. [6]School of Engineering and Applied Sciences, Harvard University, Cambridge, MA 02138, USA. [7]Mechanical and Industrial Engineering, Northeastern University, Boston, MA, USA. [8]Cardiovascular Division, Brigham and Women's Hospital, and Harvard Medical School, Boston, MA, USA.

*To whom correspondence should be sent. E-mail: don.ingber@wyss.harvard.edu

Obstruction of critical blood vessels due to thrombosis or embolism is a leading cause of death world-wide. Here we describe a biomimetic strategy that uses high shear stress caused by vascular narrowing as a targeting mechanism – in the same way platelets do–to deliver drugs to obstructed blood vessels. Microscale aggregates of nanoparticles were fabricated to break up into nano-scale components when exposed to abnormally high fluid shear stress. When coated with tissue plasminogen activator and administered intravenously in mice, these shear-activated nanotherapeutics induce rapid clot dissolution in a mesenteric injury model, restore normal flow dynamics, and increase survival in an otherwise fatal mouse pulmonary embolism model. This biophysical strategy for drug targeting, which lowers required doses and minimizes side effects while maximizing drug efficacy, offers a potential new approach for treatment of life-threatening diseases that result from acute vascular occlusion.

Disruption of normal blood flow to the heart, lung and brain is the leading cause of death and long-term adult disability in the western world (*1*). Current approaches to acute therapy for ischemic stroke, coronary infarction, and pulmonary embolism require infusion of thrombolytic drugs, which need to be administered systemically or through a catheter placed within the obstructed vessel, usually in an acute care hospital setting (*2*–*4*). To be effective, patients must receive therapy within a few hours after onset of symptoms, and the doses of clot-lysing drugs that can be administered are limited by the potential risk of bleeding as active drug is free to distribute throughout the body. To overcome these limitations, we designed a thrombolytic delivery system that targets drugs selectively to sites of flow obstruction and concentrates active drug in these regions.

Stenotic and thrombosed blood vessels exhibit unique physical characteristics that distinguish them from normal vasculature in that fluid shear stress can increase locally by one to two orders of magnitude, from below approximately 70 dyne/cm^2 in normal vessels to greater than 1,000 dyne/cm^2 in highly constricted arteries (*5*–*8*). Normal circulating platelets are locally activated by high shear stress in these regions and rapidly adhere to the adjacent surface lining of the narrowed vessels (*9*–*11*), which is a major contributing factor in development of vulnerable atherosclerotic plaques. Inspired by this natural physical mechanism of platelet targeting, we developed a therapeutic strategy that uses local high shear stress as a generic mechanism to target treatment to regions of blood vessels that are constricted by clots, stenosis or developmental abnormalities.

Our shear-activated nanotherapeutics (SA-NTs) are similar in size to natural platelets (1 to 5 μm in diameter); however, they are fabricated as aggregates of multiple smaller nanoparticles (NPs). The microscale aggregates remain intact when flowing in blood under physiological flow conditions, but break up into individual nanoscale components when exposed to high local shear stress. Because of their smaller size compared to the microscale aggregates, shear-dispersed NPs experience lower drag forces and hence, they adhere more efficiently to the surface of the adjacent blood vessel wall than the larger microaggregates (fig. S1). The efficiency of this local adhesion can be further enhanced by coating the NPs with molecules that bind to endothelial cells or relevant targets, such as fibrin clots. In this manner, high concentrations of therapeutic agents can be concentrated locally at sites of vascular occlusion or embolism by immobilizing relevant drugs or enzymes on the NPs.

The SA-NTs were produced by spray-drying concentrated solutions of biocompatible, biodegradable, poly-lactic-co-glycolic acid (PLGA 50:50, MW 17kDa) to form micrometer-sized (3.8 ± 1.6 μm) aggregates composed of small (180 ± 70 nm) NPs (Fig. 1A). Microaggregates of PLGA NPs are stable in aqueous solutions due to their hydrophobicity (*12*, *13*). But when exposed to mechanical forces that overcome the attractive forces holding the NPs together, such as hemodynamic shear stresses, the aggregates break apart (Fig. 1B), much like a wet ball of sand disperses into individual grains when rubbed in one's hands.

To determine the shear-sensitivity of this NP deployment mechanism, we used a rheometer to apply controlled shear stresses in vitro to SA-NTs fabricated from NPs labeled with a fluorescent tag. We detected an 8- to 12-fold increase in the concentration of released NPs when the level of shear reached 100 dyne/cm^2 or higher (Fig. 1C). This range of fluid shear stress is relevant in many vascular diseases. For example, computational fluid dynamics (CFD) modeling of flow within normal and stenotic human left coronary arteries based on ultrasound imaging (see Methods) (*15*, *16*) revealed that the level of shear that induce NP release in vitro is similar to that generated by a 60% lumen obstruction (Fig. 1D) whereas normal coronary vessels experience a 5-fold lower level of shear stress (~ 10 to 30 dyne/cm^2) that does not cause disruption of the SA-NTs.

To determine whether these SA-NTs can target agents selectively to stenotic regions under relevant hemodynamic flow conditions, we carried out studies in a three-dimensional (3D) microfluidic model of vascular narrowing fabricated from poly-dimethylsiloxane (PDMS) that was designed to mimic regions of living blood vessels with 90% lumen ob-

struction (Fig. 2, A and B). Based on CFD modeling, such a constriction generates ~100 fold increase in shear at the stenotic site (Fig. 2C). Perfusion of SA-NTs (100 μg/ml in PBS) through these microfluidic devices resulted in a 16-fold increase in the release of free NPs, as measured in the solution flowing downstream of the obstruction compared to fluid flowing through unobstructed microfluidic channels of similar dimensions (Fig. 2D). Moreover, fluorescence microscopic imaging confirmed that released NPs accumulated in endothelial cells cultured on the inner surface of the artificial microfluidic vessel just distal to the narrowed region whereas minimal uptake occurred in cells lining the channel prior to the constriction (Fig. 2E).

To evaluate their functional potential, we fabricated SA-NTs containing fluorescent NPs coated with the FDA-approved thrombolytic drug, tissue plasminogen activator (tPA), using biotin-streptavidin chemistry (~5×10^5 tPA molecules/micro-aggregate) and tested their ability to dissolve blood clots. To examine the general utility of this shear-targeted nanotherapeutic approach (Fig. 3A) for removal of natural clots formed endogenously in vivo, we studied the effect of bolus injection of thrombolytic SA-NTs in an established mouse arterial thrombus model in which clot formation is triggered by injuring the vessel wall by direct exposure to ferric chloride (*14*–*16*). Real-time, intravital, fluorescence microscopic studies confirmed that this treatment resulted in formation of large blood clots within minutes in injured mesenteric arteries (~100 μm diameter, normal wall shear stress ~30 dyne/cm^2) that occluded the diameter by more than 80% (Fig. 3, B and C) and caused the local shear stress to increase by more than 15-fold (~450 dyne/cm^2) in these regions, as determined using an optical Doppler velocity meter (*17*). Fluorescently-labeled tPA-carrying SA-NTs that were injected intravenously 8 min after chemical injury preferentially accumulated in the regions of clot formation, resulting in clear microscopic visualization of these lesions (Fig. 3B). In addition, the locally deployed tPA-coated NPs induced progressive surface erosion of the thrombi, with complete clearance of occlusions occurring within 5 min after SA-NT injection (Fig. 3, B and C, and movie S1). Continuous monitoring of unobstructed vessels for up to 15 min in the mesenteric bed revealed that intact microscale NP aggregates were present throughout the course of the study, indicating that circulation of the SA-NTs through the normal vasculature did not induce microaggregate disruption.

Importantly, shear-induced release of tPA-coated NPs from the SA-NTs reopened the obstructed mesenteric arteries and significantly delayed the time to vessel occlusion (29 ± 7 min with tPA-coated SA-NTs versus 12 ± 3 min with PBS), when vessel patency was monitored using intravenous injection of fluorescently-labeled platelets (~2.5% of total platelets) (Fig. 3, C and D, and movie S2). In contrast, administration of the same dose of soluble tPA (free tPA), pre-dissociated tPA-NPs, or heat-fused tPA-NP microaggregates (which do not dissociate in high shear) did not delay thrombosis in this model (Fig. 3D). Careful analysis of these results also revealed that even when a vessel is almost fully occluded, the microscale tPA-coated SA-NTs that bind to the surface of the clot can actively degrade and 'recanalize' the clot. Once this happens, flow and shear stress rapidly increase once again, and this feeds back to activate other tPA carrying SA-NTs, resulting in full clot removal (Fig. 3C and movie S2). Taken together, these results provide proof-of-principle that the SA-NT technology can be used to target clot-lysing agents to vascular occlusions, in addition to providing a way to image these lesions in real-time in situ.

To explore the potential value of the SA-NTs for treatment of life-threatening embolic occlusions, we first tested their ability to dissolve experimentally induced fibrin clots in vitro. When pre-formed fibrin clots [250 ± 150 μm diameter produced by a water-in-oil emulsion technique (*18*)] were injected into microfluidic channels that contained constricted regions (80 μm high, 500 μm wide), the fibrin emboli lodged in the devices and partially obstructed flow in the channels (Fig. 4A). When SA-NTs (100 μg/ml) carrying tPA (50 ng/ml) were infused at physiological flow rates through the clot-occluded microfluidic channels, the shear-dispersed fluorescent tPA-coated NPs accumulated at the surface of the artificial emboli, progressively dissolving the clots and reducing their size by one half within an hour of treatment (Fig. 4A and movie S3). In contrast, treatment with soluble tPA at the same concentration and flow conditions had negligible effects (<5% reduction in clot size) (Fig. 4B).

Next, we tested the ability of this shear-activated tPA delivery system to reverse the effects of acute pulmonary embolism in an ex vivo whole mouse lung ventilation-perfusion model. A solution containing the pre-formed fibrin clots similar to those tested in the microfluidic channel were infused (0.1 ml/min for ~5 min; 1×10^3 clots/ml) through the pulmonary artery of the perfused lung. Occlusion of pulmonary blood vessels by multiple microemboli (Fig. 4C) caused the pulmonary artery pressure to increase by about 3-fold compared to its normal value (30 versus 8 mm Hg) (Fig. 4E). We then perfused tPA-coated SA-NTs (100 μg/ml microscale aggregates containing NPs coated with 50 ng/ml tPA) through the pulmonary artery at a physiological flow rate (0.5 ml/min). Fluorescence microscopic analysis of tissue sections again confirmed that the tPA-NPs localized selectively at regions of vascular occlusion, producing a greater than 25-fold increase in accumulation of NPs at these sites, (Figs. 4, C and D). Progressive lysis of the emboli by the tPA-NPs resulted in normalization of pulmonary artery pressure levels within 1 hour in this ex vivo model (Fig. 4E). In contrast, perfusion of soluble tPA at the same concentration as that delivered on the injected tPA-coated NPs (50 ng/ml), or even at a ten times higher dose (500 ng/ml), failed to produce any significant response (Fig. 4F). In fact, similar clot-lysing effects and hemodynamic changes were only observed when we administered a hundred times higher concentration of soluble tPA under identical flow conditions (Fig. 4F); this dose in mice (~2 mg/kg) is comparable to the therapeutic dose commonly used in humans (~1 mg/kg).

We then studied pulmonary embolism in living mice by infusing smaller preformed fluorescent fibrin clots (< 70 μm; ~1,000 clots) into the jugular vein of anesthetized mice, which accumulate in peripheral blood vessels in the lungs, as previously described (*19*). SA-NTs coated with tPA were then infused either immediately after injection of emboli, or 30 min after they formed. Quantitation of the total area of fluorescent emboli visualized in the lungs using computerized image analysis confirmed that administration of the tPA-coated SA-NTs resulted in reduction of both total clot area and clot number by more than 60% when administered immediately after injection of emboli, and by more than 30% when infused one half hour after embolism (Fig. S2).

To further examine the potential clinical relevance of our approach for treatment of life-threatening acute massive embolism, we infused a solution containing larger fibrin clots (150 ± 80 μm diameter; ~ 100/injection), which accumulate in the main pulmonary arteries (*19*) much as they do in humans with pulmonary embolism, and the mice were then immediately infused with tPA-coated SA-NTs or with carrier fluid for 45 min. All control animals died within 1 hour after infusion of the clots (0% survival, n = 7, Fig. 4G), whereas more than 80% of the treated mice survived (6 out of 7), and none of these SA-NTs-treated animals displayed any visible symptoms of respiratory distress.

The major potential advantage of the SA-NTs is their ability to enhance the safety of thrombolytic therapies by significantly reducing the drug dose required to be effective, as demonstrated by the ability of SA-NTs to clear pulmonary emboli when coated with a tPA dose ~1/100th that required for induction of similar clot-lysing effects by free tPA. SA-NTs also could help to minimize unwanted bleeding and neurotoxicity because they are cleared rapidly from the circulation (80% clearance in 5 min) (fig. S3), and due to their larger size, they should not diffuse as easily into injured tissues as free tPA does. Additionally, it is important

to note that we have not observed any abnormal bleeding in mice during the extensive surgical manipulations that were involved in our pulmonary embolism and mesenteric artery occlusion models. Nevertheless, before advancing these SA-NTs toward clinical studies in the future, finer control over the size of the microscale aggregates and their pharmacokinetics will be required to ensure that they safely pass through all microvessels and are sustained in the circulation at effective levels (*20*). Alternative methods to link tPA to NPs (e.g., direct conjugation by amine-carboxylate coupling or coupling based on biocompatible heterobifunctional PEG linkers; (*21, 22*) also will need to be explored to avoid immune responses associated with streptavidin/biotin conjugation and to increase conjugation efficiency as well as optimize tPA activity.

A previously described thrombo-prophylaxis strategy based on coupling plasminogen activators to carrier erythrocytes has shown promising results in preventing thrombosis in various animal models (*23–25*). The SA-NTs described here can potentially be used to prevent formation of thrombi that partially occlude vascular flow, as occurs for example when a stable atherosclerotic plaque is transformed into a life-threatening vulnerable plaque. However, in contrast to the erythrocyte delivery approach, which is limited to prevention of nascent clot formation, the shear-activated drug targeting strategy also offers the ability to treat and dissolve pre-existing fibrin clots, such as those found in patients with stroke and myocardial infarction as well as atherosclerosis. In this proof of principle study, we focused on SA-NTs coupled to a thrombolytic agent, tPA, which has high affinity for fibrin and thus, they were efficiently delivered to fibrin clots (fig. S1). In addition, these tPA-coated SA-NTs were loaded with a fluorescent dye that also concentrated at vascular occlusion sites. In the future it should be possible to design and fabricate SA-NTs containing various drugs or imaging agents for localized treatment and real-time visualization in a variety of pathologies associated with vascular obstruction.

In summary, these findings illustrate how nanoengineering approaches inspired by pathophysiological mechanisms can be used to develop safer and more effective therapeutic strategies. In contrast to drug targeting mechanisms that focus on expression of distinct molecular species that can vary between tissues or patients, shear stress increases as a function of narrowing of the lumen diameter in all patients, regardless of the cause or location of obstruction, thus offering a robust and broadly applicable targeting strategy. With further refinement, the shear-activated drug targeting nanotechnology described here might, for example, allow the immediate administration of clot-busting drugs to patients suspected to have life-threatening clots in the brain, lung or other vital organs by emergency technicians or other care-givers, even before the patient has reached a hospital setting.

References and Notes

1. C. J. L. Murray, A. D. Lopez, Mortality by cause for eight regions of the world: Global Burden of Disease Study. *Lancet* **349**, 1269 (1997). doi:10.1016/S0140-6736(96)07493-4 Medline
2. T. J. Ingall *et al*., Findings from the reanalysis of the NINDS tissue plasminogen activator for acute ischemic stroke treatment trial. *Stroke* **35**, 2418 (2004). doi:10.1161/01.STR.0000140891.70547.56 Medline
3. T. G. Kwiatkowski *et al*.; National Institute of Neurological Disorders and Stroke Recombinant Tissue Plasminogen Activator Stroke Study Group, Effects of tissue plasminogen activator for acute ischemic stroke at one year. *N. Engl. J. Med.* **340**, 1781 (1999). doi:10.1056/NEJM199906103402302 Medline
4. L. R. Wechsler, Intravenous thrombolytic therapy for acute ischemic stroke. *N. Engl. J. Med.* **364**, 2138 (2011). doi:10.1056/NEJMct1007370 Medline
5. J. Strony, A. Beaudoin, D. Brands, B. Adelman, *Am. J. Physiol. Heart Circ. Physiol.* **265**, H1787 (1993).
6. D. M. Wootton, D. N. Ku, Fluid mechanics of vascular systems, diseases, and thrombosis. *Annu. Rev. Biomed. Eng.* **1**, 299 (1999). doi:10.1146/annurev.bioeng.1.1.299 Medline
7. J. M. Siegel, C. P. Markou, D. N. Ku, S. R. Hanson, A scaling law for wall shear rate through an arterial stenosis. *J. Biomech. Eng.* **116**, 446 (1994). doi:10.1115/1.2895795 Medline
8. D. L. Bark, Jr., D. N. Ku, Wall shear over high degree stenoses pertinent to atherothrombosis. *J. Biomech.* **43**, 2970 (2010). doi:10.1016/j.jbiomech.2010.07.011 Medline
9. Z. M. Ruggeri, J. N. Orje, R. Habermann, A. B. Federici, A. J. Reininger, Activation-independent platelet adhesion and aggregation under elevated shear stress. *Blood* **108**, 1903 (2006). doi:10.1182/blood-2006-04-011551 Medline
10. W. S. Nesbitt *et al*., A shear gradient-dependent platelet aggregation mechanism drives thrombus formation. *Nat. Med.* **15**, 665 (2009). doi:10.1038/nm.1955 Medline
11. S. Goto *et al*., Enhanced shear-induced platelet aggregation in acute myocardial infarction. *Circulation* **99**, 608 (1999). doi:10.1161/01.CIR.99.5.608 Medline
12. M. J. Santander-Ortega, A. B. Jódar-Reyes, N. Csaba, D. Bastos-González, J. L. Ortega-Vinuesa, Colloidal stability of pluronic F68-coated PLGA nanoparticles: a variety of stabilisation mechanisms. *J. Colloid Interface Sci.* **302**, 522 (2006). doi:10.1016/j.jcis.2006.07.031 Medline
13. M. Santander-Ortega, N. Csaba, M. Alonso, J. Ortega-Vinuesa, D. Bastos-González, Stability and physicochemical characteristics of PLGA, PLGA:poloxamer and PLGA:poloxamine blend nanoparticles. *Colloids Surf. A Physicochem. Eng. Asp.* **296**, 132 (2007). doi:10.1016/j.colsurfa.2006.09.036
14. H. Ni *et al*., Persistence of platelet thrombus formation in arterioles of mice lacking both von Willebrand factor and fibrinogen. *J. Clin. Invest.* **106**, 385 (2000). doi:10.1172/JCI9896 Medline
15. A. K. Chauhan *et al*., Systemic antithrombotic effects of ADAMTS13. *J. Exp. Med.* **203**, 767 (2006). doi:10.1084/jem.20051732 Medline
16. W. Bergmeier *et al*., The role of platelet adhesion receptor GPIbalpha far exceeds that of its main ligand, von Willebrand factor, in arterial thrombosis. *Proc. Natl. Acad. Sci. U.S.A.* **103**, 16900 (2006). doi:10.1073/pnas.0608207103 Medline
17. P. S. Frenette *et al*., Platelet-endothelial interactions in inflamed mesenteric venules. *Blood* **91**, 1318 (1998). Medline
18. R. Gref *et al*., Biodegradable long-circulating polymeric nanospheres. *Science* **263**, 1600 (1994). doi:10.1126/science.8128245 Medline
19. J. C. Murciano *et al*., Platelets inhibit the lysis of pulmonary microemboli. *Am. J. Physiol. Lung Cell. Mol. Physiol.* **282**, L529 (2002). Medline
20. J. A. Straub, D. E. Chickering, T. G. Hartman, C. A. Gloff, H. Bernstein, AI-700 pharmacokinetics, tissue distribution and exhaled elimination kinetics in rats. *Int. J. Pharm.* **328**, 35 (2007). doi:10.1016/j.ijpharm.2006.07.052 Medline
21. M. Di Marco *et al*., Overview of the main methods used to combine proteins with nanosystems: absorption, bioconjugation, and encapsulation. *Int. J. Nanomedicine* **5**, 37 (2010). Medline
22. S. Rana, Y. C. Yeh, V. M. Rotello, Engineering the nanoparticle-protein interface: applications and possibilities. *Curr. Opin. Chem. Biol.* **14**, 828 (2010). doi:10.1016/j.cbpa.2010.10.001 Medline
23. J. C. Murciano *et al*., Prophylactic fibrinolysis through selective dissolution of nascent clots by tPA-carrying erythrocytes. *Nat. Biotechnol.* **21**, 891 (2003). doi:10.1038/nbt846 Medline
24. K. Danielyan *et al*., Cerebrovascular thromboprophylaxis in mice by erythrocyte-coupled tissue-type plasminogen activator. *Circulation* **118**, 1442 (2008). doi:10.1161/CIRCULATIONAHA.107.750257 Medline
25. K. Ganguly *et al*., Fibrin affinity of erythrocyte-coupled tissue-type plasminogen activators endures hemodynamic forces and enhances fibrinolysis in vivo. *J. Pharmacol. Exp. Ther.* **316**, 1130 (2006). doi:10.1124/jpet.105.093450 Medline
26. C. E. Astete, C. M. Sabliov, Synthesis and characterization of PLGA nanoparticles. *J. Biomater. Sci. Polym. Ed.* **17**, 247 (2006). doi:10.1163/156856206775997322 Medline
27. J. C. Sung *et al*., Formulation and pharmacokinetics of self-assembled rifampicin nanoparticle systems for pulmonary delivery. *Pharm. Res.* **26**, 1847 (2009). doi:10.1007/s11095-009-9894-2 Medline
28. A. U. Coskun *et al*., Reproducibility of coronary lumen, plaque, and vessel wall reconstruction and of endothelial shear stress measurements in vivo in humans. *Catheter. Cardiovasc. Interv.* **60**, 67 (2003). doi:10.1002/ccd.10594 Medline

29. Y. Xia, G. M. Whitesides, SOFT LITHOGRAPHY. *Annu. Rev. Mater. Sci.* **28**, 153 (1998). doi:10.1146/annurev.matsci.28.1.153
30. S. L. Diamond, Engineering design of optimal strategies for blood clot dissolution. *Annu. Rev. Biomed. Eng.* **1**, 427 (1999). doi:10.1146/annurev.bioeng.1.1.427 Medline
31. C. K. Lam, T. Yoo, B. Hiner, Z. Liu, J. Grutzendler, Embolus extravasation is an alternative mechanism for cerebral microvascular recanalization. *Nature* **465**, 478 (2010). doi:10.1038/nature09001 Medline
32. D. Huh *et al*., Reconstituting organ-level lung functions on a chip. *Science* **328**, 1662 (2010). doi:10.1126/science.1188302 Medline

Acknowledgments: We thank D. Huh, K. Roberts and R.F. Valentini for helpful comments and K. Johnson, D. Stanton for help with the graphics. This work was supported by a U.S. Department of Defense Breast Cancer Innovator award BC074986 (to D.E.I.), grants from Novartis Pharmaceuticals Inc. and Boston Scientific Inc. (to C.L.F. and A.U.C.), and the Wyss Institute for Biologically Inspired Engineering at Harvard University. N.K. is a recipient of a Wyss Technology Development Fellowship. Harvard University and the authors (DEI, NK, MK) have filed two patents related to this work: (i) Shear-Activated Nanotherapeutics for Drug Targeting and (iii) Shear Controlled Release for Stenotic Lesions and Thrombolytic Therapies.

Supporting Online Material
www.sciencemag.org/cgi/content/full/science.1217815/DC1
Materials and Methods
Figs. S1 to S3
References (*26*–*32*)
Movies S1 to S3

13 December 2011; accepted 14 June 2012
Published online 28 June 2012
10.1126/science.1217815

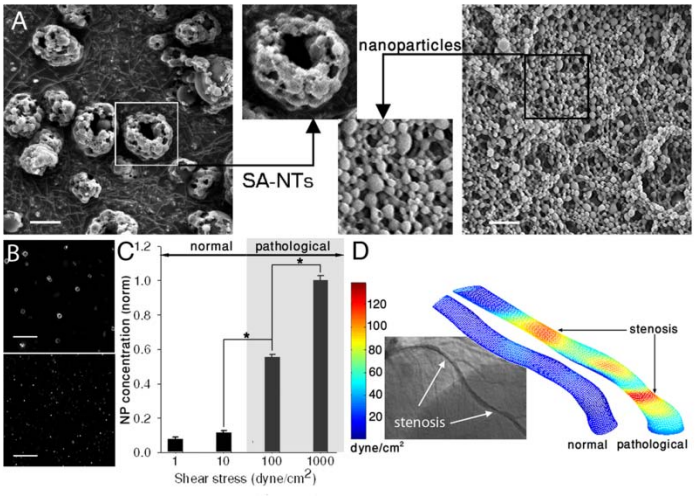

Fig. 1. Microscale SA-NTs disperse into nanoparticles only when exposed to pathological shear stresses. (**A**) Scanning electron micrographs of the microscale (~2-5 μm) SA-NTs (left) and the PLGA nanoparticles (NPs; ~180 nm) used to produce them (right) (bar, 2 μm). (**B**) Fluorescence micrographs demonstrating intact SA-NTs (top) and NPs dispersed after their exposure to 1,000 dyne/cm^2 for 10 min using a rheometer (bottom) (bar, 10 μm). (**C**) Quantification of release of fluorescent NPs from the SA-NTs as a function of shear revealed that exposure to pathological levels of shear (≥100 dyne/cm^2 for 1 min) caused large increase in the breakup of the microscale aggregates into NPs compared to physiological levels of shear (1 or 10 dyne/cm^2) (*P < 0.005). (**D**) CFD simulations comparing fluidic shear stress in a normal coronary artery (left) and a stenotic vessel with a 60% lumen obstruction (right); left inset shows the corresponding angiogram of the stenotic left coronary artery in a 63 year old male patient.

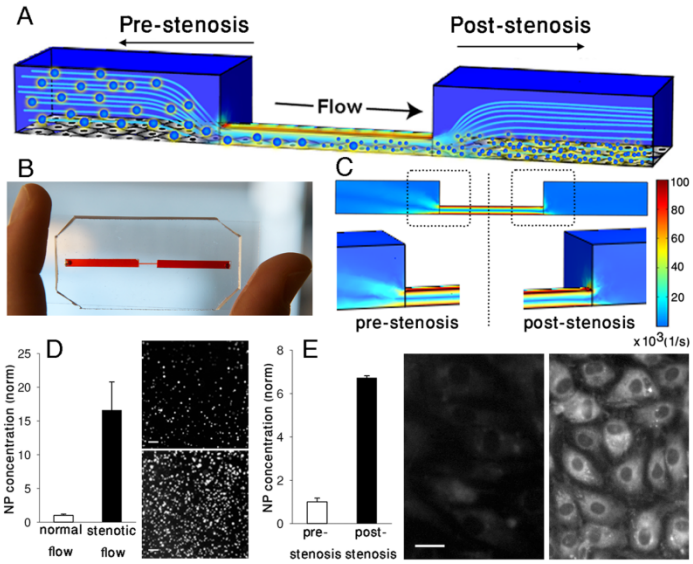

Fig. 2. Shear-induced dissociation of SA-NTs and nanoparticle targeting under hemodynamic conditions in microfluidic devices. (**A**) A microfluidic vascular stenosis model showing how SA-NTs (large spheres) should remain intact in the pre-stenotic region, but then break up into NPs (small spheres) when they flow through a constriction (90% lumen occlusion) and can accumulate in endothelial cells lining the bottom of the channel. (**B**) A photograph of the microdevice that mimics vascular stenosis fabricated in PDMS. (**C**) CFD simulations of the microfluidic device shown in B demonstrating that a physiological inlet shear rate of 1,000 s^{-1} (10 dyne/cm^2) upstream from the constriction increases to a pathological level of ~100,000 s^{-1} [1,000 dyne/cm^2] in the region displaying 90% lumen occlusion. (**D**) Graph shows a greater than 10-fold increase in release of fluorescent NPs from SA-NTs when they are perfused through the channel shown in B compared with flow through an unconstricted channel (*P < 0.005). Fluorescent micrographs compare the NPs collected in the outflow from the control channel (top) versus the constricted channel (bottom) (bar, 2 μm). (**E**) Graph demonstrates that many more fluorescent NPs accumulate in endothelial cells lining the downstream area (post-stenosis) of the constriction relative to an upstream area (p < 0.005). Fluorescence microscopic images show cells from regions before (left) and after (right) the constriction (bar, 20 μm).

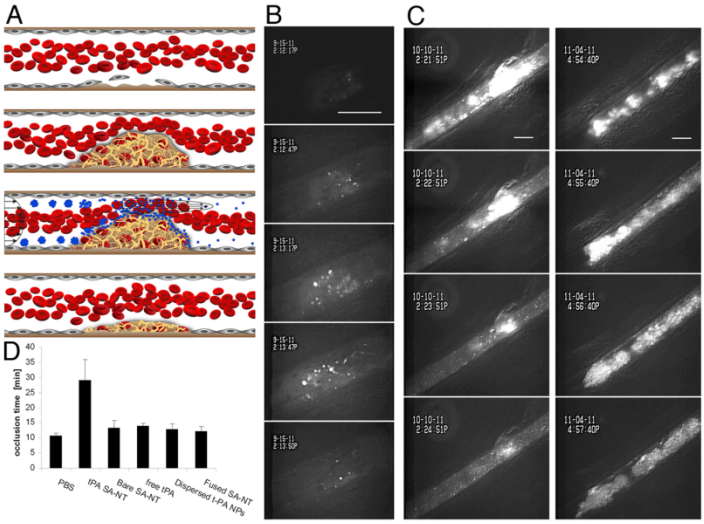

Fig. 3. Shear-targeting of a thrombolytic drug in a mouse arterial thrombosis model using SA-NTs. (**A**) Schematic of the experimental strategy. Ferric chloride injury initiates formation of a thrombus (top) that grows to partially obstruct blood flow (upper middle). Intraveneously injected SA-NTs dissociate into NPs at the thrombus site due to the rise in local shear stress (lower middle). Accumulation of tPA-coated NPs and binding to the clot at the occlusion site progressively dissolve the obstruction (bottom). (**B**) Sequential intravital fluorescence microscopic images of a thrombus in a partially occluded mesenteric artery recorded over a 5 min period beginning after bolus injection of fluorescent tPA-coated SA-NTs (1 mg NPs; 50 ng tPA) 8 min after injury initiation (bar, 100 μm). Note that the NPs accumulate at the clot, first visualizing its location and then demonstrating clearance of the clot within 5 min after injection at the bottom (also see Supplementary Movie S1). (**C**) Sequence of intravital fluorescence microscopic images recorded over a 5 min period showing fluorescently-labeled platelets accumulated within a forming thrombus that partially occludes a mesenteric artery 8 min after injury. Thrombosis is then treated with injection of either tPA-carrying SA-NTs (50 ng tPA) (left) or PBS (right) (bar, 100 μm). Note that the clot on the left is greatly reduced in size within 5 min after SA-NTs injection (also Supplementary Movie S2), whereas the control vessel on the right fully occludes over the same time period. (**D**) Graph showing that a bolus injection of SA-NTs carrying 50 ng tPA (tPA-SA-NT) significantly delayed the time to full vascular occlusion in FeCl-injured vessels (***$P < 0.0005$), whereas administration of the same concentration of soluble tPA (free tPA), uncoated SA-NTs (bare SA-NT), tPA-coated NPs that were artificially dissociated from SA-NTs prior to injection (dispersed tPA-NPs), and heat-fused NP microaggregates with tPA coating that do not dissociate (fused SA-NT) did not produce any significant delay in thrombosis.

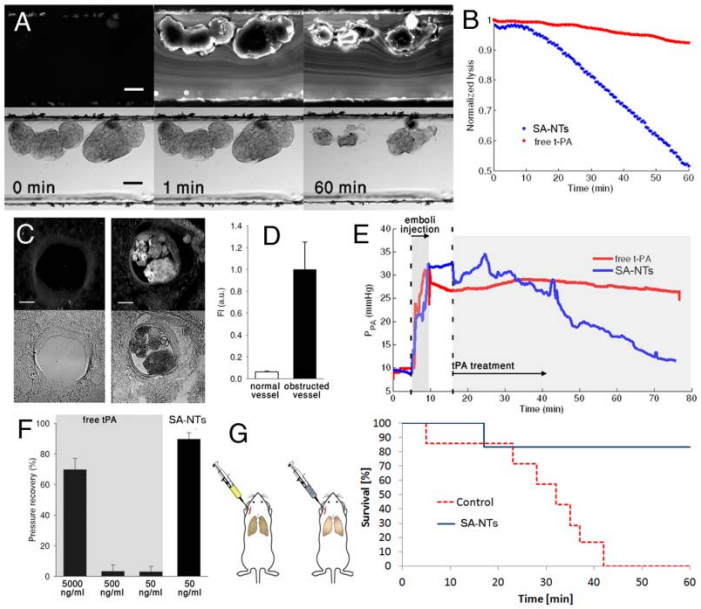

Fig. 4. Shear-targeting of a thrombolytic drug to vascular emboli in vitro and therapeutic delivery in a mouse pulmonary embolism model. (**A**) Time lapse fluorescence (top) and bright field (bottom) views of artificial microemboli (~ 250 μm) in a microfluidic channel before (0 min) and 1 or 60 min after injection of SA-NTs coated with tPA (50 ng/ml) showing progressive lysis of the clots over time (also see Supplementary S3 movie; bar, 100 μm). (**B**) Graph showing enhanced emboli lysis kinetics induced by tPA-coated SA-NTs (50 ng/ml, blue line) compared to soluble tPA (red line). (**C**) Fluorescence (top) and phase contrast (bottom) views of histological sections of normal (left) versus obstructed (right) pulmonary arteries showing local accumulation of fluorescent NPs within the obstructing emboli in a mouse ex vivo lung ventilation-perfusion model (bar, 100 μm). (**D**) Graph showing almost a 20-fold increase ($P < 0.005$) in accumulation of fluorescent NPs in regions of obstructed versus non-obstructed vessels, as detected by microfluorimetry. (**E**) Real-time measurements of pulmonary artery pressure in the ex vivo pulmonary embolism model showing that the tPA-coated SA-NTs (blue line) reversed pulmonary artery hypertension within approximately 1 hour, whereas the same concentration (50 ng/ml) of free tPA was ineffective (red line). (**F**) Graph showing that tPA carrying SA-NTs normalize pulmonary artery pressure within an hour, whereas the same concentration of free tPA (50 ng/ml) or a 10 times higher dose (500 ng/ml) did not reduce pulmonary artery pressure ($^*P < 0.005$); only a 100-fold higher dose (5,000 ng/ml) produced similar effects. (**G**) Survival curve showing that almost all (86%) of the mice injected with the tPA-coated SA-NTs survived, whereas all control mice died within 45 min after injection of fibrin clots that caused acute emboli formation.

Supplementary Material for

Shear-Activated Nanotherapeutics for Drug Targeting to Obstructed Blood Vessels

Netanel Korin, Mathumai Kanapathipillai, Benjamin D. Matthews, Marilena Crescente, Alexander Brill, Tadanori Mammoto, Kaustabh Ghosh, Samuel Jurek, Sidi A. Bencherif, Deen Bhatta, Ahmet U. Coskun, Charles L. Feldman, Denisa D. Wagner, Donald E. Ingber*

*To whom correspondence should be sent. E-mail: don.ingber@wyss.harvard.edu

Published 5 July 2012 on *Science* Express
DOI: 10.1126/science.1217815

This PDF file includes:

Other Supplementary Material for this manuscript includes the following:
(available at www.sciencemag.org/cgi/content/full/science.1217815/DC1)

Movies S1 to S3

MATERIALS AND METHODS

Nanoparticle preparation - Nanoparticles (NPs) were prepared from PLGA (50:50, 17kDa, acid terminated; Lakeshore Biomaterials, AL) using a simple solvent displacement method (*26*). The fluorescent hydrophobic dye, coumarin-6, was included in the NPs to enable visualization and quantitation in this study. Briefly, 1 mg/ml of polymer was dissolved with 0.1 wt% coumarin in dimethyl sulfoxide (DMSO, Sigma, MO), dialyzed against water at room temperature, and the nanoparticles were allowed to form by solvent displacement and subsequent self-assembly in aqueous solution. The size distribution and morphology of the formed NPs were characterized using Dynamic Light Scattering (DLS), Scanning Electron Microscopy (SEM) and Transmission Electron Microscopy (TEM).

Fabrication of SA-NTs - The PLGA NPs were centrifuged and concentrated to a 10 mg/ml suspension in water and 1 mg/ml L-leucine (Spectrum Chemicals & Laboratory Products, CA) was added. NP aggregates (SA-NTs) were prepared by a spray-drying technique using a Mobile Minor spray dryer (Niro, Inc.; Columbia, MD). The aqueous leucine-NP suspension was infused separately from the organic phase (ethanol) at a ratio of 1.5:1 and mixed in-line immediately prior to atomization (*27*). The inlet temperature was 80°C and the liquid feed rate was 50 ml/min; gas flow rate was set at 25 g/min and nozzle pressure was 40 psi. Spray dried powders were collected in a container at the outlet of the cyclone. SA-NTs suspensions were formed by reconstituting the powders in water at desired concentrations. Aggregate suspensions were filtered through 20 μm filters to filter out any oversized aggregates; centrifugation (2000g for 5 min) followed by washing also was used to remove single unbound NPs. DLS was used to determine the size of the NPs in dilute solutions using a zeta particle size analyzer (Malvern instruments, UK) operating with a HeNe laser, 173° back scattering detector. Samples were prepared at 1 mg/ml concentration in PBS buffer at pH 7.4. Data collection and analysis was performed with Malvern instrument software.

Functionalization with tPA - NP aggregates (1 mg/ml) were pre-activated with 1-ethyl-3-(3-dimethylaminopropyl) (EDC) and Sulfo-NHS (N-hydroxysulfosuccinimide) at 1:5:10 (PLGA:EDC:NHS) molar ratio in 0.1 M MES buffer, pH 6.0 for 1 hour. The reaction mixture was then centrifuged and washed twice with PBS and subsequently reacted with linker NH_2-PEG-biotin (Thermofisher Scientific, Rockford, IL) at a 1:10 molar ratio in PBS, pH 7.4 at room temperature for 2 hours. The aggregates were then centrifuged and washed twice and reacted with streptavidin (Thermofisher Scientific, Rockford, IL) for 15 minutes at room temperature. The aggregates were purified by repeated centrifugation and washing to remove any unreacted reagents. Separately, human tissue plasminogen activator (tPA, Cell Sciences, MA) was functionalized with biotin using linker NHS-PEG-biotin in PBS at room temperature for 2 hours at a 1:10 molar ratio (*23*). The functionalized tPA was then reacted with the strepatvidin-biotin-aggregates for 30 min at room temperature. The tPA functionalized NP aggregates tPA were then purified by centrifugation and washing; the amount of tPA conjugated to the aggregates was determined by fluorescence spectrometry. Briefly, aggregates were dissolved in 1M NaOH under stirring at 37°C for ~ 6h until a clear polymer solution was obtained. The amount of tPA

(TRITC-labeled, Cell Sciences, MA) in the polymer solution was then measured at 594 nm. Activity of tPA coated particles was confirmed using a fluorometric tPA activity assay (SensoLyte,AnaSpec,CA); after immobilization, tPA-coated NPs retained ~70% of the activity exhibited by soluble tPA. SEM of the aggregated nanoparticles was performed using a Zeiss FESEM Supra55vP (Center for Nanosystems (CNS), Harvard University). Samples were mounted on carbon tape adhesive substrates and sputter coated with gold under vacuum using a sputter coater (Center for Nanosystems(CNS), Harvard University). The coated NP aggregates were imaged at 4 kV using an in-lens detector at 9 mm working distance.

Rheometer Shearing Assay - A solution of SA-NTs (5 mg/ml in 8% Polyvinylpyrrolidone solution) was sheared for 1 min using a 20 mm cone & plate configuration in a Rheometer (AR-G2 TA Instruments, DE). The solutions were then collected, filtered through a 0.45 micron filter (Millipore, MA) to remove large microscale aggregates from NPs and diluted 1:3 with water. The fluorescence intensity of these NP suspensions was measured using a PTI QM40 Fluorometer (PTI-FL) (Photon Technology International, NJ) and normalized relative to the highest shear level (1,000 dyne/cm^2) value.

Computational Fluid Dynamics (CFD) simulations - CFD simulations for the microfluidic channels were performed using the software package Comsol 3.5 (Comsol, USA), based on a finite element method. We considered the flow to be steady and incompressible, and assumed a no-slip boundary condition at the walls and the fluid medium (PBS) to have a constant density of 1000 kg/m^3 and viscosity of 1 mPa-sec. CFD simulations of IVUS reconstructed blood vessel were preformed as previously described (*28*).

Microfluidic Models of Vascular Stenosis- Microchannels mimicking vascular constriction used for studies on microemboli formation were prepared from poly-dimethylsiloxane (PDMS) using conventional soft lithography (*29*). A master mold was prepared by aligning 80 micron layers designed using a CAD program and formed using a cutter plotter (CE5000, Graphtec, CA). The device contained a region (160 μm high x 400 μm wide x 10 mm long) with a 90% constriction relative to upstream and downstream channel regions (each: 640 μm high x 2 mm wide x 20 mm long). The PDMS channels were sealed with a glass microslide (170 μm thick) using plasma bonding. In some studies, solutions of SA-NTs (5 ml, 100 ug/ml) were recirculated through microfluidic devices with 90% occlusion or without any constriction using a peristaltic pump (ISM 834C, Ismatec SA, Switzerland). Flow rate was adjusted to obtain a wall shear stress of 10 dyne/cm^2 at the unconstructed channels. The suspensions were collected after 20 minutes of flow and filtered through a sub-micron (0.45um) filter. The fluorescent intensity of the collected NP suspensions was measured using a spectrometer (Photon Technology International, NJ) and normalized relative to the unconstricted channel value. For studies on release of NPs and their binding to endothelial cells in stenotic regions, the microfluidic devices were sterilized using oxygen plasma and coated with fibronectin (50ug/ml @ 30 min) to support cell adhesion. Bovine aortic endothelial cells (Lonza,MD) were introduced to the microchannel and allowed to adhere under static conditions (2 hr at 37°C). The devices were then placed in a tissue culture incubator and medium (EGM®-MV BulletKit, Lonza, MD) was infused (50 μL/hr) using a syringe pump (Braintree Scientific, Braintree, MA).

The endothelial cells were cultured in the devices for 3- 4 day until a continuous cell monolayer was formed. A solution containing SA-NTs (10 μg/ml) was then infused for 10 min through the device at a flow rate which produces a wall shear stress of ~10 dyne/cm^2 in the unconstructed channel. Unattached particles were flushed away by infusing water through the channels at the same flow rate for 5 min. Phase contrast and fluorescence microscopic images of cells and bound NPs in regions proximal upstream and downstream to the constriction were acquired using a Zeiss microscope. The averaged fluorescence intensity of cell-associated coumarin-loaded NPs obtained from these views was used to evaluate the difference in NP accumulation between pre- and post stenotic regions.

Microfluidic Models of Vascular Embolism - Microfluidic devices with a narrowed cross-sectional area (80 μm high x 0.5 mm wide s 200 mm long) were fabricated using soft lithography as described above. Fibrin clots formed as described below that were infused into the main channel lodged and obstructed the flow in these smaller channels. A solution of tPA or tPA coated SA-NTs was infused at a flow rate corresponding to a shear stress of 10 dyne/cm^2 in an unobstructed channel. Prior to infusion of the tPA solutions, bovine plasminogen (Cell Sciences, MA) was added to a final concentration of 2.2 μM (*30*). During the fibrinolysis process, the fibrin clot sizes were monitored in real-time (images acquired every 30 sec) on an inverted Zeiss microscope.

Experimental Fibrin Emboli- Fibrin clots were formed by adding $CaCl_2$ (20 mM) and human α-thrombin (1 units/ml final concentrations, Enzyme Research Laboratories, IN) to human fibrinogen (5 mg/ml, Enzyme Research Laboratories,IN), as previously described (*23, 31*). This solution was immediately added drop-wise to a solution of canola oil with Span-80 (0.05%). The emulsion was mixed at 350 rpm for 4 hr and centrifuged (500g, 5min), followed by repeated washing in ethanol and water. The diameter of the resulting fibrin beads was determined by optical microscopy to be ~ 250 μm. By adjusting the mixing speed in the described protocol, fibrin beads of smaller defined sizes were produced.

Ex-vivo Mouse Pulmonary Embolism Model - 6-8 week-old C57BL/6 male mice (Jackson Laboratory, Bar Harbor, ME) were weighed and anesthetized with Avertin (200 mg/kg IP). The trachea was incised via surgical tracheotomy, and cannulated with a blunted 22G stainless steel needle tip. The lungs were subsequently ventilated at a rate of 60 breaths/min, with a Peak Inspiratory Pressure (Pip) of 10 cm H_2O and a Positive End Expiratory Pressure (Peep) of 3 cm H_2O with compressed air using a mouse ventilator (VCM-R, Hugo Sachs Elektroniks, Germany). *Ex vivo* ventilation and perfusion of the mouse lung was performed using an IL1 *ex vivo* mouse lung ventilation-perfusion system (Harvard Apparatus, Natick, MA), (*32*). Following initiation of mechanical ventilation, the chest was opened via thoracotomy, and heparin (100 IU) was injected into the right ventricle. After 30 seconds, the thoracic aorta and superior vena cava were cut and the animal exsanguinated. A suture was placed around the pulmonary artery and aorta. Cannulae made from polyethylene tubing (PE90 (0.86 mm ID, 1.7 mm OD)) were placed in the pulmonary artery (PA) and left atrium (LA), and lungs were perfused with RPMI-1640 with 4% Bovine Albumin (ProbuminTM Reagent Grade, Billerica, MA) and 0.7 g NaCl/500 ml via a roller pump (ISM 834C, Ismatec SA, Switzerland) set at a constant flow rate of 0.5 ml/min in a recirculating system with a system volume of 6 ml. Perfusate and lung temperatures were

maintained at 37°C by housing the entire *ex-vivo* ventilation perfusion system inside a standard cell incubator without CO_2 (Forma Scientific, Ohio). Humidity was maintained in the range of 90-95%. Pulmonary arterial and left atrial pressures and airway flow and pressures were recorded with dedicated Type 379 vascular pressure and DLP2.5 flow and MPX Type 399/2 airway pressure transducers and TAM-A amplifiers (Hugo Sachs Elektroniks, Germany). Vascular pressures were zeroed at the mid lung level prior to each experiment and recorded using Polyview16© software (Grass Technologies, West Warwick, RI).

Prior to injection of experimental fibrin clots (prepared as above), the measured pressures were allowed to stabilize and remain stable for a period of more than 10 minutes. A solution of fibrin clots suspended in perfusion medium was infused at a flow rate of 0.1ml/min and mixed with the regular perfusion line entering the pulmonary artery. The fibrin clot suspension was infused until the pulmonary artery pressure increased to ~ three-fold higher than the baseline. The system was then allowed to equilibrate and remain stable for at least 10 minutes. Next, tPA-coated SA-NTs or free soluble tPA was added to the main perfusion line and circulated through the perfusion system. As in the microfluidic device experiments, when tPA was perfused, plasminogen was added to obtain a final concentration of 2.2 μM. Pulmonary artery and vein pressures were acquired continuously during the perfusion period. At the end of each experiment, lungs were perfused with 4% paraformaldehyde, and prepared for sectioning by incubating in 4% paraformaldehyde, then sucrose and OCT. All experimental animal protocols were approved by the Institutional Animal Care and Use Committee at Children's Hospital Boston and Harvard Medical School.

In vivo Mouse Pulmonary Embolism Model (PE)- 6-8 week-old male C57BL/6 mice (Jackson Laboratory, Bar Harbor, ME) were weighed and anesthetized with Avertin (200 mg/kg IP). A ventro-lateral incision was made in the neck and a jugular vein catheter (PE10 tubing (0.28 mm ID, 0.61 mm OD, BD Biosciences) was inserted through which a solution containing preformed fibrin clots was infused using a syringe pump (Braintree Scientific Inc). Different size of emboli were used: in the acute PE model, large fibrin clots were used (150 ± 80 micron; 0.1 ml @ 1 x 10^3 clots/ml over 2 minutes) , while in the peripheral PE model smaller emboli were injected (30 ± 25 micron; 0.1 ml@ 1 x 10^4 clots/ml over 2 minutes). Animals were subsequently injected via the jugular vein catheter with tPA coated SA-NTs (1 mg particles/ml in PBS @ 3 ul/min; 500 ng tPA total) or with carrier fluid for 45 minutes. Following the treatment period, animals were further monitored for an additional 15 min. Animal core temperature was maintained at 37°C using a temperature regulated heating lamp. At the conclusion of the experiments animals were euthanized and their lungs and organs prepared for histology using standard techniques. Prior to histology, intact lungs were placed under an upright fluorescent microscope and emboli located in peripheral blood vessel were observed. Brightfield and fluorescent images of the lungs were captured .The size distribution of emboli observed in the peripheral blood vessels was determined using a threshold and performing size analysis on the fluorescent images (ImageJ) on areas which were in focus in their corresponding brightfield image.

Mouse Ferric Chloride Arterial Injury Model- A previously described model was used with minor modifications(*16*). In brief, male C57BL/6 mice (3–4 weeks old) were anesthetized with 2.5 % tribromoethanol (0.15ml/10g) and injected with fluorescently labeled platelets (calcein

Red/Orange, ~1 x10^9 platelets/kg). An incision was made through the abdominal wall to expose the mesentery and arterioles (~100 μm in diameter) were visualized using a Zeiss Axiovert 135-inverted microscope (objectives: 10x and 32x, Carl Zeiss MicroImaging, Inc.) and recorded on videotape. Whatman filter paper saturated with FeCl3 (10%) solution was applied topically for 5 min, which caused denudation of the endothelium. 100 ul of PBS solutions with either SA-NTs coated with tPA (50 ng tPA, 1mg), bare SA-NTs, soluble tPA (50ng), pre-dispersed t-PA SA-NTs into NPs (pre-sheared using 30 min flow in microfluidic devices with wall shear stress of 1,000 dyne/cm^2, followed by sonication @60W, 2 min), unbreakable shear insensitive SA-NTs coated with t-PA (NPs in SA-NTs were fused by incubation in 60°C for >4hr) or PBS alone were administrated through the retro-orbital plexus of the eye, 7-8 min after removal of the ferric chloride filter paper. Following this bolus injection, the vessels were monitored until full occlusion occurred (blood flow stopped) and lasted for more than 10 seconds. The shear rate was calculated using an optical Doppler velocity meter (Microcirculation Research Institute, Texas A&M College of Medicine, College Station, TX)(*17*). One arteriole was chosen per mouse.

Adhesion of NPs and Microaggregates under Flow - Microfluidic devices contain a narrowed channel (80 μm high x 2 mm wide x 200 mm long) were fabricated using soft lithography as described above. A glass slide coated with a thin dry layer of fibrin (< 1 μm thick) was bonded to the bottom of the channel. Fluorescent NPs (200nm) and microparticles (2μm) were coated with tPA as detailed above. A solution of the coated NPs or microaggregates (100ug/ml) was infused in the channel at a flow rate corresponding to a wall shear stress of 10 dyne/cm^2 for 15 min. At the end of the experiment, the channels were washed with water at the same flow rate for >10 min. Fluorescence microscopy images were taken and analyzed to evaluate the area covered by particles.

Biodistribution of Particles in mice- 100 μl of SA-NTs or dispersed NPs solution (5mg/ml) was bolus injected through the jugular vein of anesthetized male 6-8 week-old C57BL/6 mice. 5 minutes post injection animals were killed and the major organs (liver, lungs, spleen and kidney) were harvested. The organs were homogenized in DMSO and mixed for 30 min on a shaker. The mixed solutions were then centrifuged (10,000g for 10 min) and the supernatant was collected. The fluorescence intensity of the supernatant was measured using PTI QM40 Fluorometer (PTI-FL), (Photon Technology International, NJ) at 460/515nm excitation and emission. Organs from control mice were similarly processed, and the baseline organ autofluorescence values measured were subtracted from the treated group measurements. A calibration curve built using SA-NTs solutions of different concentrations was used to correlate the tissue measurements to their injected dose (ID) values. Accumulation of particles in the blood was estimated by fluorescent intensity measurements of blood samples.

SUPPLEMENTARY FIGURES

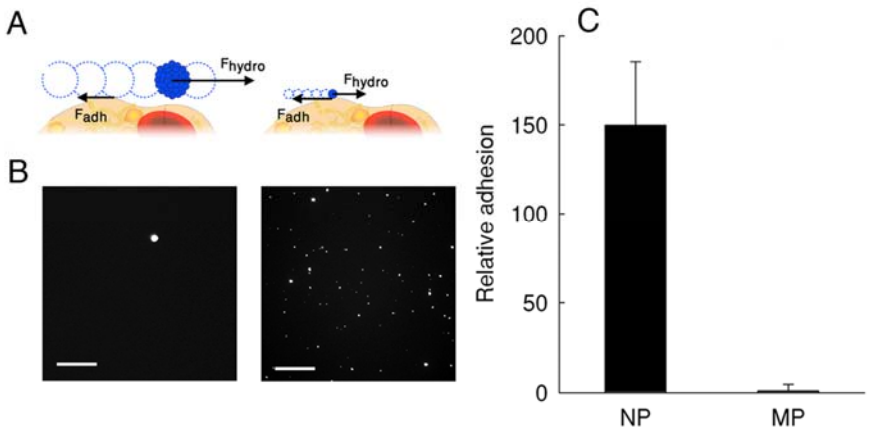

Fig. S1. Enhanced adhesion of nanoparticles compared to microparticles under flow. **A)** Nanoparticles (NPs) experience lower hemodynamic forces (F_{hydro}) due to their smaller size ($F_{hydro} \approx r^2$) compared to micrometer-sized particles, causing them to adhere more efficiently to the surrounding vascular wall and surface endothelium, while the larger particles that experience higher drag forces are pulled away by fluid flow.
B) Fluorescence microscopic images showing much higher level of binding of the NPs (average size 200 nm) at the left, compared to the microaggregates (average size 2 μm) at the right. Both NP solutions were coated with tPA (50 ng/mg) and infused at the same concentration (100 μg/ml in PBS) for 15 min through a fibrin-coated 80 μm channel, which produces the same normal shear stress of 10 dyne/cm^2 (bar, 10 μm). **C)** Quantitation of the surface adhesion of tPA-coated NPs compared to microaggregates corresponding to the normal conditions described in **B**.

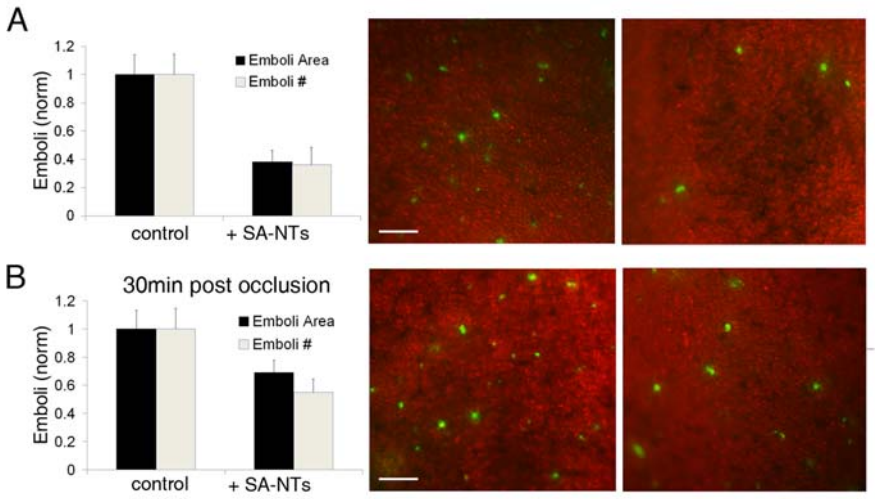

Fig. S2. Induction of emboli lysis in vivo in the mouse pulmonary embolism model using t-PA-coated SA-NTs. Graphs (left) and fluorescence microscopic images (right) showing that intravenous administration with tPA-coated SA-NTs (+SA-NTs) immediately **(A)** or 30 min **(B)** after infusion of fluorescent fibrin clots (< 70 μm) and induction of multiple small emboli results in a significant ($p < 0.05$) reduction in both the total area covered by emboli and the number of emboli in the lungs compared to controls injected with PBS. Data are presented normalized relative to control results at the left; green dots in images at right indicates fluorescent emboli; red represents a brightfield image of the lung (bar, 150 μm).

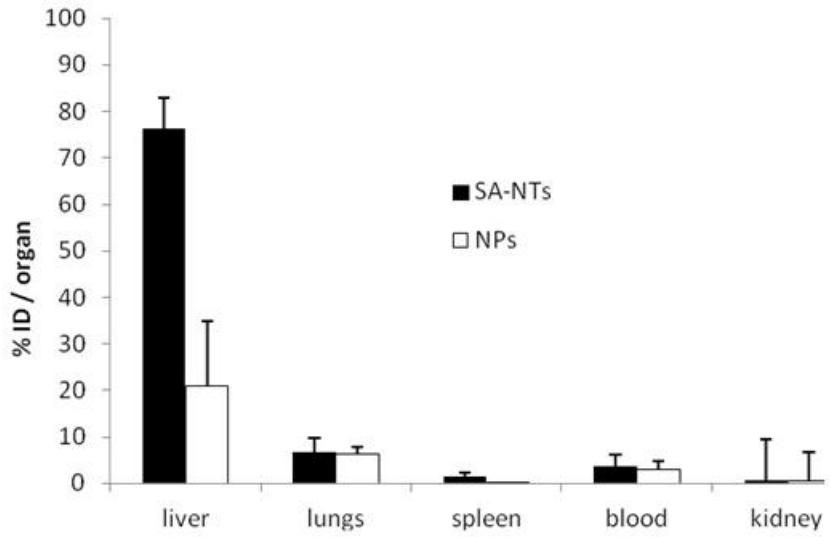

Fig. S3. Biodistribution of SA-NTs and NPs in mice measured 5 min after intravenous administration. The SA-NTs or NPs (5 mg/ml) were injected as a bolus (100 ul) through the jugular vein of mice, and 5 min later the major organs responsible for clearance of particulates (liver, lung, spleen, and kidney) and the blood were harvested. The percentage of the Injection Dose (ID) contained within each organ (%ID/organ) was estimated based on fluorescence measurements of the harvested tissues. Note that the SA-NTs and NPs exhibited different clearance efficiencies with a much great proportion of the SA-NTs being cleared (primarily by the liver) within 5 min after injection.

SUPPLEMENTARY MOVIE CAPTIONS

Movie S1. Intravital microscopy movie of fluorescently-labeled tPA-coated SA-NTs, following bolus injection, flowing through a partly occluded mesenteric artery. Note that the clot becomes coated and impregnated with the fluorescent NPs, which remove the clot and reopen the vessel within 5 minutes after injection.

Movie S2. Intravital microscopy movie of fluorescent-labeled platelets in a partly occluded ferric chloride injured mesenteric artery following bolus injection of tPA-coated SA-NTs. Note that the clot is removed and the vessel is reopened within 5 minutes after injection.

Movie S3. This time-lapse movie shows SA-NTs coated with tPA (50 ng/ml) flowing over fibrin clots that partially occlude a microfluidic channel to model vascular embolism. Note that the emboli become coated and impregnated with the fluorescent NPs (left), which progressively dissolve the clots over the 1 hour period of recording, as shown in the phase contrast view (right).

References and Notes

1. C. J. L. Murray, A. D. Lopez, Mortality by cause for eight regions of the world: Global Burden of Disease Study. *Lancet* **349**, 1269 (1997). doi:10.1016/S0140-6736(96)07493-4 Medline

2. T. J. Ingall *et al*., Findings from the reanalysis of the NINDS tissue plasminogen activator for acute ischemic stroke treatment trial. *Stroke* **35**, 2418 (2004). doi:10.1161/01.STR.0000140891.70547.56 Medline

3. T. G. Kwiatkowski *et al*.; National Institute of Neurological Disorders and Stroke Recombinant Tissue Plasminogen Activator Stroke Study Group, Effects of tissue plasminogen activator for acute ischemic stroke at one year. *N. Engl. J. Med.* **340**, 1781 (1999). doi:10.1056/NEJM199906103402302 Medline

4. L. R. Wechsler, Intravenous thrombolytic therapy for acute ischemic stroke. *N. Engl. J. Med.* **364**, 2138 (2011). doi:10.1056/NEJMct1007370 Medline

5. J. Strony, A. Beaudoin, D. Brands, B. Adelman, *Am. J. Physiol. Heart Circ. Physiol.* **265**, H1787 (1993).

6. D. M. Wootton, D. N. Ku, Fluid mechanics of vascular systems, diseases, and thrombosis. *Annu. Rev. Biomed. Eng.* **1**, 299 (1999). doi:10.1146/annurev.bioeng.1.1.299 Medline

7. J. M. Siegel, C. P. Markou, D. N. Ku, S. R. Hanson, A scaling law for wall shear rate through an arterial stenosis. *J. Biomech. Eng.* **116**, 446 (1994). doi:10.1115/1.2895795 Medline

8. D. L. Bark, Jr., D. N. Ku, Wall shear over high degree stenoses pertinent to atherothrombosis. *J. Biomech.* **43**, 2970 (2010). doi:10.1016/j.jbiomech.2010.07.011 Medline

9. Z. M. Ruggeri, J. N. Orje, R. Habermann, A. B. Federici, A. J. Reininger, Activation-independent platelet adhesion and aggregation under elevated shear stress. *Blood* **108**, 1903 (2006). doi:10.1182/blood-2006-04-011551 Medline

10. W. S. Nesbitt *et al*., A shear gradient-dependent platelet aggregation mechanism drives thrombus formation. *Nat. Med.* **15**, 665 (2009). doi:10.1038/nm.1955 Medline

11. S. Goto *et al*., Enhanced shear-induced platelet aggregation in acute myocardial infarction. *Circulation* **99**, 608 (1999). doi:10.1161/01.CIR.99.5.608 Medline

12. M. J. Santander-Ortega, A. B. Jódar-Reyes, N. Csaba, D. Bastos-González, J. L. Ortega-Vinuesa, Colloidal stability of pluronic F68-coated PLGA nanoparticles: a variety of stabilisation mechanisms. *J. Colloid Interface Sci.* **302**, 522 (2006). doi:10.1016/j.jcis.2006.07.031 Medline

13. M. Santander-Ortega, N. Csaba, M. Alonso, J. Ortega-Vinuesa, D. Bastos-González, Stability and physicochemical characteristics of PLGA, PLGA:poloxamer and PLGA:poloxamine blend nanoparticles. *Colloids Surf. A Physicochem. Eng. Asp.* **296**, 132 (2007). doi:10.1016/j.colsurfa.2006.09.036

14. H. Ni *et al*., Persistence of platelet thrombus formation in arterioles of mice lacking both von Willebrand factor and fibrinogen. *J. Clin. Invest.* **106**, 385 (2000). doi:10.1172/JCI9896 Medline

15. A. K. Chauhan *et al*., Systemic antithrombotic effects of ADAMTS13. *J. Exp. Med.* **203**, 767 (2006). doi:10.1084/jem.20051732 Medline

16. W. Bergmeier *et al*., The role of platelet adhesion receptor GPIbalpha far exceeds that of its main ligand, von Willebrand factor, in arterial thrombosis. *Proc. Natl. Acad. Sci. U.S.A.* **103**, 16900 (2006). doi:10.1073/pnas.0608207103 Medline

17. P. S. Frenette *et al*., Platelet-endothelial interactions in inflamed mesenteric venules. *Blood* **91**, 1318 (1998). Medline

18. R. Gref *et al*., Biodegradable long-circulating polymeric nanospheres. *Science* **263**, 1600 (1994). doi:10.1126/science.8128245 Medline

19. J. C. Murciano *et al*., Platelets inhibit the lysis of pulmonary microemboli. *Am. J. Physiol. Lung Cell. Mol. Physiol.* **282**, L529 (2002). Medline

20. J. A. Straub, D. E. Chickering, T. G. Hartman, C. A. Gloff, H. Bernstein, AI-700 pharmacokinetics, tissue distribution and exhaled elimination kinetics in rats. *Int. J. Pharm.* **328**, 35 (2007). doi:10.1016/j.ijpharm.2006.07.052 Medline

21. M. Di Marco *et al*., Overview of the main methods used to combine proteins with nanosystems: absorption, bioconjugation, and encapsulation. *Int. J. Nanomedicine* **5**, 37 (2010). Medline

22. S. Rana, Y. C. Yeh, V. M. Rotello, Engineering the nanoparticle-protein interface: applications and possibilities. *Curr. Opin. Chem. Biol.* **14**, 828 (2010). doi:10.1016/j.cbpa.2010.10.001 Medline

23. J. C. Murciano *et al*., Prophylactic fibrinolysis through selective dissolution of nascent clots by tPA-carrying erythrocytes. *Nat. Biotechnol.* **21**, 891 (2003). doi:10.1038/nbt846 Medline

24. K. Danielyan *et al*., Cerebrovascular thromboprophylaxis in mice by erythrocyte-coupled tissue-type plasminogen activator. *Circulation* **118**, 1442 (2008). doi:10.1161/CIRCULATIONAHA.107.750257 Medline

25. K. Ganguly *et al*., Fibrin affinity of erythrocyte-coupled tissue-type plasminogen activators endures hemodynamic forces and enhances fibrinolysis in vivo. *J. Pharmacol. Exp. Ther.* **316**, 1130 (2006). doi:10.1124/jpet.105.093450 Medline

26. C. E. Astete, C. M. Sabliov, Synthesis and characterization of PLGA nanoparticles. *J. Biomater. Sci. Polym. Ed.* **17**, 247 (2006). doi:10.1163/156856206775997322 Medline

27. J. C. Sung *et al*., Formulation and pharmacokinetics of self-assembled rifampicin nanoparticle systems for pulmonary delivery. *Pharm. Res.* **26**, 1847 (2009). doi:10.1007/s11095-009-9894-2 Medline

28. A. U. Coskun *et al*., Reproducibility of coronary lumen, plaque, and vessel wall reconstruction and of endothelial shear stress measurements in vivo in humans. *Catheter. Cardiovasc. Interv.* **60**, 67 (2003). doi:10.1002/ccd.10594 Medline

29. Y. Xia, G. M. Whitesides, SOFT LITHOGRAPHY. *Annu. Rev. Mater. Sci.* **28**, 153 (1998). doi:10.1146/annurev.matsci.28.1.153

30. S. L. Diamond, Engineering design of optimal strategies for blood clot dissolution. *Annu. Rev. Biomed. Eng.* **1**, 427 (1999). doi:10.1146/annurev.bioeng.1.1.427 Medline

31. C. K. Lam, T. Yoo, B. Hiner, Z. Liu, J. Grutzendler, Embolus extravasation is an alternative mechanism for cerebral microvascular recanalization. *Nature* **465**, 478 (2010). doi:10.1038/nature09001 Medline

32. D. Huh *et al*., Reconstituting organ-level lung functions on a chip. *Science* **328**, 1662 (2010). doi:10.1126/science.1188302 Medline